

# On the Generalized CP Symmetry, One Zero Texture in Neutrino Mass Matrix and Neutrinoless Double Beta Decay

Priya\*, Simran Arora† and B. C. Chauhan‡

*Department of Physics and Astronomical Science, Central University of Himachal Pradesh, Dharamshala (HP) 176215, India*

## Abstract

In this study, we explore the impact of one zero textures on the neutrino mass matrix, focusing on their ability to constrain neutrino parameters such as mixing angles, Dirac and Majorana phases, and mass eigenstates. We investigate one zero textures within the framework of generalized CP symmetry associated with the complex tribimaximal matrix. By combining these approaches, we derive predictive neutrino mass matrices and elucidate correlations between various parameters. Additionally, we analyze neutrinoless double beta decay in the context of one zero textures, in the light of current and future experimental data. Our analysis shows that sum of the three neutrino masses in the inverted hierarchy is inconsistent with cosmological bounds provided by the Planck data,  $\Sigma m_i < 0.12$  eV. We also include bounds from the DESI/SDSS+Pantheon+DES-SN dataset ( $\Sigma m_i < 0.17$  eV) in the  $\Lambda$ CDM + Fluid DR +  $\sum m_\nu$  model at 95% confidence level, which completely disfavors the inverted hierarchy. Our findings highlight the enhanced predictability and testability of neutrino mass models that incorporate generalized CP symmetry.

Keywords: Generalized CP Symmetry, Neutrino Mass Matrix, Complex Tribimaximal Matrix, Neutrinoless Double Beta Decay.

## 1 Introduction

The Standard Model (SM) of particle physics is the theory that describes three of the four known fundamental forces in the universe (electromagnetic, weak, and strong interactions, excluding gravity) and classifies all known elementary particles with massless neutrinos. Its remarkable success strongly indicates that the SM will remain an excellent approximation to nature at distance scales as small as  $10^{-18}$  m [1]. The signatures of solar and atmospheric neutrino oscillations detected by the Super-Kamioka Neutrino Detection Experiment (Super-Kamiokande) [2] and the Sudbury Neutrino Observatory (SNO) [3] later validated by the Kamioka Liquid Scintillator Antineutrino Detector (KamLAND) experiment [4], which confirmed that neutrinos possess a very small mass, thereby revealing the limitations of the SM. After measurement of the reactor mixing angle  $\theta_{13}$  from the experiments Daya Bay [5], RENO [6] and Double Chooz [7], all the three mixing angles ( $\theta_{12}$ ,  $\theta_{23}$ ,  $\theta_{13}$ ), solar mass squared difference, i.e.  $\Delta m_{\text{solar}}^2$  and magnitude of atmospheric mass squared difference, i.e.  $\Delta m_{\text{atm}}^2$  have been measured successfully with considerable precision [8]. The determination of neutrino mass hierarchy, matter-antimatter asymmetry, the nature of neutrinos, and CP violation in the lepton sector still remain unsolved mysteries. Therefore, these issues are the primary focus of upcoming experiments. The best fit values with errors ( $\sigma$ 's) of mixing angles and mass squared differences are listed in Table 1 [9].

---

\*kashyappriya963@gmail.com

†009simranarora@gmail.com

‡bcawake@hpcu.ac.in

S.No.	Neutrino Parameters	Best Fit ( $1\sigma$ )	( $3\sigma$ )
1	$\Delta m_{\text{solar}}^2/10^{-5} \text{ eV}^2$	$7.41_{-0.20}^{+0.21}$	6.82 - 8.03
2	$\Delta m_{\text{atm}}^2/10^{-3} \text{ eV}^2$	$2.507_{-0.027}^{+0.026}$	2.427 - 2.590
3	$\theta_{12}/^\circ$	$33.41_{-0.72}^{+0.75}$	31.31 - 35.74
4	$\theta_{13}/^\circ$	$8.58_{-0.11}^{+0.11}$	8.23 - 8.91
5	$\theta_{23}/^\circ$	$42.3_{-0.9}^{+1.1}$	39 - 51

Table 1: Best fit values of neutrino parameters with  $1\sigma$  and  $3\sigma$  ranges taken from [9].

The confirmation of nonzero neutrino masses from neutrino oscillation experiments is the first significant evidence of physics beyond the Standard Model [10]. The discovery of  $\nu_\mu \rightarrow \nu_e$  appearance by T2K in 2013 [11], later confirmed by the NuMI Off-Axis  $\nu_e$  Appearance (NO $\nu$ A) experiment [12], holds significant importance providing the way for exploring three-flavor effects. In the framework of three active neutrinos, mass and flavor eigenstates are related by the  $3 \times 3$  mixing matrix, commonly referred as the Pontecorvo-Maki-Nakagawa-Sakata (PMNS) matrix. The lepton mixing matrix is defined by nine parameters: three mass eigenstates, three mixing angles, and three phases, i.e., one Dirac type CP phase and two Majorana type CP phases (the two additional phases present in the Majorana case do not affect oscillations) [13]. The PMNS matrix in the standard parametrization [14] is

$$U_{PMNS} = \begin{pmatrix} \cos \theta_{12} \cos \theta_{13} & \sin \theta_{12} \cos \theta_{13} & \sin \theta_{13} e^{-i\delta} \\ -\cos \theta_{23} \sin \theta_{12} - \cos \theta_{12} \sin \theta_{13} \sin \theta_{23} e^{i\delta} & \cos \theta_{12} \cos \theta_{23} - \sin \theta_{12} \sin \theta_{13} \sin \theta_{23} e^{i\delta} & \cos \theta_{13} \sin \theta_{23} \\ \sin \theta_{12} \sin \theta_{23} - \cos \theta_{12} \sin \theta_{13} \cos \theta_{23} e^{i\delta} & -\cos \theta_{12} \sin \theta_{23} - \sin \theta_{12} \sin \theta_{13} \cos \theta_{23} e^{i\delta} & \cos \theta_{13} \cos \theta_{23} \end{pmatrix} P. \quad (1)$$

Here,  $\theta_{12}$ ,  $\theta_{13}$ ,  $\theta_{23}$  are the mixing angles,  $\delta$  is the Dirac CP phase and matrix P is a diagonal matrix representing a phase matrix consisting two Majorana phases. The tribimaximal (TBM) mixing pattern is one of the most extensively studied lepton mixing schemes, often explored through the application of flavor symmetries [15–18]. A key prediction of the TBM mixing pattern is that the reactor mixing angle,  $\theta_{13}$ , should be zero. Additionally, the atmospheric mixing angle is expected to be maximal, i.e.,  $\theta_{23} = \frac{\pi}{4}$ . Furthermore, TBM mixing predicts a specific value for the solar mixing angle,  $\theta_{12} = \sin^{-1} \left( \frac{1}{\sqrt{3}} \right)$  given as

$$U_{\text{TBM}} = \begin{pmatrix} \frac{\sqrt{2}}{\sqrt{3}} & \frac{1}{\sqrt{3}} & 0 \\ -\frac{1}{\sqrt{6}} & \frac{1}{\sqrt{3}} & \frac{1}{\sqrt{2}} \\ \frac{1}{\sqrt{6}} & \frac{1}{\sqrt{3}} & -\frac{1}{\sqrt{2}} \end{pmatrix}. \quad (2)$$

The Majorana phases will be disappeared if neutrinos are Dirac particles. We can express the lepton mass matrix as

$$m_\nu = U^* \text{diag}(m_1, m_2, m_3) U^\dagger. \quad (3)$$

The mixing matrix  $U$  can exhibit specific patterns due to residual flavor symmetries of the neutrino mass matrix  $m_\nu$  [19]. These residual symmetries occur when  $m_\nu$  remains invariant under certain non-trivial transformations  $G_i$  [20]

$$G_i = U d_i U^\dagger, \quad i = 1, 2, 3, 4, \quad (4)$$

where the  $d_i$  are given as

$$d_1 = \text{diag}(1, -1, -1), \quad d_2 = \text{diag}(-1, 1, -1), \quad d_3 = \text{diag}(-1, -1, 1), \quad d_4 = \text{diag}(1, 1, 1). \quad (5)$$

The exploration of residual flavor symmetries in the neutrino mass matrix has led to the study of other types of symmetries, including the generalized remnant CP transformation. Unlike residual flavor symmetries, which leave the neutrino mass matrix  $m_\nu$  unchanged, these generalized CP transformations convert  $m_\nu$  into its complex conjugate  $m_\nu^*$ . These transformations are represented by  $X_i$  and are connected to the lepton mixing matrix  $U$  by the relation

$$X_i = U d_i U^T \quad \text{for } i = 1, 2, 3, 4. \quad (6)$$

The imposition of any two of these CP symmetries results in modified TBM mixing patterns, each associated with a single residual flavor symmetry. Specifically, the action of two CP transformations,  $X_i X_j^*$ , is equivalent to a flavor symmetry transformation  $G_k$ , where  $i, j$ , and  $k$  are cyclic permutations of  $\{1, 2, 3\}$ . This equivalence is crucial as it allows the lepton mixing matrix to be derived from residual CP symmetries [21]. Moreover, using generalized CP symmetries, rather than just flavor symmetries, constrains the Majorana CP phases, making this approach particularly effective as compared to the flavor symmetries.

In addition to residual flavor and remnant CP symmetries, alternative approaches such as imposing texture zeros [22–27], vanishing cofactors [28–30], hybrid textures [31–35], or equalities [36] among the neutrino mass matrix elements have also been explored to explain neutrino masses and mixings. Assuming that neutrinos are Majorana particles and the charged lepton mass matrix is diagonal, texture zeros in the neutrino mass matrix represent one of the simplest frameworks consistent with current and future neutrino experimental data. The combined use of flavor symmetry and texture zeros or vanishing cofactors in constructing neutrino mass matrix has led to highly predictive models. The another promising approach involves imposing texture zeros in conjunction with generalized CP symmetries.

In this work, we aim to explore the implications of one zero textures within the framework of generalized CP symmetries  $X_1$  and  $X_2$ . By combining these two approaches, we have constructed a more predictive model for the neutrino mass matrix. Specifically, we have examined patterns of one zero textures that are consistent with the symmetries imposed by  $X_1$  and  $X_2$ . The presence of the complex tribimaximal matrix,  $G_i \neq X_i$ , allows us to distinguish between flavor symmetry and generalized CP symmetry. The preservation of flavor symmetries is thoroughly explained in [37]. The  $G_i = X_i$  case with texture zeros is examined in detail in [38]. In our analysis, we focus only on the  $G_1$  and  $G_2$  flavor symmetries, however  $G_3$  corresponds to a reactor mixing angle equal to zero, which is experimentally excluded.

Our analysis considers the effect of these patterns on the values of neutrino masses, mixing angles, and CP-violating phases. The rest part of the paper is organized as - the forms of the neutrino mixing matrix and mass matrix for the  $X_1$  and  $X_2$  CP symmetries are derived in Section 2, where we also detail the methodology for mixing angles and CP-violating phases. We explore the implications of imposing one zero condition within the  $X_1$  and  $X_2$  CP symmetries and assess the impact on neutrino parameters in light of current and future experimental data. One zero textures is discussed in Section 3. The results of this study are summarized in Section 4, with conclusions presented in Section 5.

## 2 Generalized CP symmetries

The mixing matrix  $U$  shows specific patterns due to residual flavor symmetries of the neutrino mass matrix  $m_\nu$ . These residual symmetries occur when  $m_\nu$  remains invariant under certain non-trivial transformations  $G_i$ , such that

$$G_i^T m_\nu G_i = m_\nu \quad \text{for } i = 1, 2, 3, 4. \quad (7)$$

Here,  $G_4$  is the trivial identity matrix, and we can check that

$$G_i^2 = 1, \quad \text{and} \quad G_i G_j = G_j G_i = G_k \quad \text{with } i \neq j \neq k \neq 4.$$

The residual flavor symmetry of the Majorana neutrino mass matrix corresponds to the Klein group, isomorphic to  $Z_2 \times Z_2$ . Both quark and lepton mass matrices can exhibit simultaneous remnant flavor and CP symmetries. The explicit form of these symmetries is constrained by the experimentally observed lepton mixing matrix. In this section, we explore detailed structure of the remnant flavor and CP symmetries, examining their parametrization by combining both symmetries and how they contribute to the phenomenology of neutrino masses and mixing. For the Majorana neutrinos, the most general form of the corresponding neutrino mass matrix in the charged lepton diagonal basis is

$$m_\nu^{\text{TBM}} = U_{\text{TBM}} \text{diag}(m_1, m_2, m_3) U_{\text{TBM}}^T, \quad (8)$$

such that

$$m_\nu^{\text{TBM}} = \frac{1}{6} \begin{pmatrix} 4m_1 + 2m_2 & -2m_1 + 2m_2 & -2m_1 + 2m_2 \\ -2m_1 + 2m_2 & m_1 + 2m_2 + 3m_3 & m_1 + 2m_2 - 3m_3 \\ -2m_1 + 2m_2 & m_1 + 2m_2 - 3m_3 & m_1 + 2m_2 + 3m_3 \end{pmatrix}. \quad (9)$$

The neutrino mass matrix represented by Eqn. 9 remains invariant under the following residual flavor transformations given as

$$G_1^{\text{TBM}} = \frac{1}{3} \begin{pmatrix} 1 & -2 & -2 \\ -2 & -2 & 1 \\ -2 & 1 & -2 \end{pmatrix}, \quad G_2^{\text{TBM}} = \frac{1}{3} \begin{pmatrix} -1 & 2 & 2 \\ 2 & -1 & 2 \\ 2 & 2 & -1 \end{pmatrix}, \quad G_3^{\text{TBM}} = - \begin{pmatrix} 1 & 0 & 0 \\ 0 & 0 & 1 \\ 0 & 1 & 0 \end{pmatrix}. \quad (10)$$

In other words, the neutrino mass matrix  $m_\nu^{\text{TBM}}$  satisfies

$$(G_i^{\text{TBM}})^T m_\nu^{\text{TBM}} G_i^{\text{TBM}} = m_\nu^{\text{TBM}},$$

for  $i = 1, 2, 3$ .

## Complex TBM Matrix

Here, we explore into the complex tribimaximal(cTBM) matrix, incorporating non-zero Majorana phases [40]. Such that the cTBM matrix is given as

$$U_{cTBM} = \begin{pmatrix} \frac{\sqrt{2}}{\sqrt{3}} & \frac{e^{-i\rho}}{\sqrt{3}} & 0 \\ -\frac{e^{i\rho}}{\sqrt{6}} & \frac{1}{\sqrt{3}} & \frac{e^{-i\sigma}}{\sqrt{2}} \\ \frac{e^{i(\rho+\sigma)}}{\sqrt{6}} & -\frac{e^{i\sigma}}{\sqrt{3}} & \frac{1}{\sqrt{2}} \end{pmatrix}. \quad (11)$$

This cTBM mixing matrix predicts the same mixing angles as the usual real TBM pattern in Eqn. 2, though the Majorana phases are non-vanishing. The exploration of residual flavor symmetries in the neutrino mass matrix  $m_\nu$  has extended to include generalized CP symmetries, which transform the mass matrix into its complex conjugate  $m_\nu^*$ . These transformations are represented by  $X_i$  and are connected to the lepton mixing matrix  $U$  by the relation presented in Eqn. 6. These symmetries are often studied in the context of finite discrete groups like  $\Delta(6n^2)$  [41], which naturally lead to trimaximal mixing patterns. This approach can yield specific predictions for the Dirac and Majorana CP phases, influencing ongoing experimental searches for neutrino oscillation parameters and neutrinoless double-beta decay ( $0\nu\beta\beta$ ) observables [21]. The generalized CP symmetry  $X_i$  is present in  $m_\nu$  if

$$X_i^T m_\nu X_i = m_\nu^*. \quad (12)$$

The four CP symmetry matrices  $X_{1,2,3,4}$  associated with the cTBM mixing pattern are

$$X_i = U_{cTBM} d_i U_{cTBM}^T, \quad (13)$$

where  $d_{1,2,3,4}$  are diagonal matrices as given in Eqn. 5. Thus, the four CP symmetries are given in matrix form as

$$\begin{aligned} X_1 &= \frac{1}{6} \begin{pmatrix} 4 - 2e^{-2i\rho} & -2e^{-i\rho} - 2e^{i\rho} & 2e^{i(\rho+\sigma)} + 2e^{-i(\rho+\sigma)} \\ -2e^{-i\rho} - 2e^{i\rho} & -2 + e^{2i\rho} - 3e^{-2i\sigma} & -3e^{-i\sigma} - e^{i(2\rho+\sigma)} + 2e^{i\sigma} \\ 2e^{i(\rho+\sigma)} + 2e^{-i(\rho+\sigma)} & -3e^{-i\sigma} - e^{i(2\rho+\sigma)} + 2e^{i\sigma} & -3 + e^{2i(\rho+\sigma)} - 2e^{2i\sigma} \end{pmatrix}, \\ X_2 &= \frac{1}{6} \begin{pmatrix} -4 + 2e^{-2i\rho} & 2e^{-i\rho} + 2e^{i\rho} & -2e^{i(\rho+\sigma)} - 2e^{-i(\rho+\sigma)} \\ 2e^{-i\rho} + 2e^{i\rho} & 2 - e^{2i\rho} - 3e^{-2i\sigma} & -3e^{-i\sigma} + e^{i(2\rho+\sigma)} - 2e^{i\sigma} \\ -2e^{i(\rho+\sigma)} - 2e^{-i(\rho+\sigma)} & -3e^{-i\sigma} + e^{i(2\rho+\sigma)} - 2e^{i\sigma} & -3 - e^{2i(\rho+\sigma)} + 2e^{2i\sigma} \end{pmatrix}, \\ X_3 &= \frac{1}{6} \begin{pmatrix} -4 - 2e^{-2i\rho} & -2e^{-i\rho} + 2e^{i\rho} & -2e^{i(\rho+\sigma)} + 2e^{-i(\rho+\sigma)} \\ -2e^{-i\rho} + 2e^{i\rho} & -2 - e^{2i\rho} + 3e^{-2i\sigma} & 3e^{-i\sigma} + e^{i(2\rho+\sigma)} + 2e^{i\sigma} \\ -2e^{i(\rho+\sigma)} + 2e^{-i(\rho+\sigma)} & 3e^{-i\sigma} + e^{i(2\rho+\sigma)} + 2e^{i\sigma} & 3 - e^{2i(\rho+\sigma)} - 2e^{2i\sigma} \end{pmatrix}, \\ X_4 &= \frac{1}{6} \begin{pmatrix} 4 + 2e^{-2i\rho} & 2e^{-i\rho} - 2e^{i\rho} & 2e^{i(\rho+\sigma)} - 2e^{-i(\rho+\sigma)} \\ 2e^{-i\rho} - 2e^{i\rho} & 2 + e^{2i\rho} + 3e^{-2i\sigma} & 3e^{-i\sigma} - e^{i(2\rho+\sigma)} - 2e^{i\sigma} \\ 2e^{i(\rho+\sigma)} - 2e^{-i(\rho+\sigma)} & 3e^{-i\sigma} - e^{i(2\rho+\sigma)} - 2e^{i\sigma} & 3 + e^{2i(\rho+\sigma)} + 2e^{2i\sigma} \end{pmatrix}. \end{aligned} \quad (14)$$

The CP symmetries corresponding to the “standard” real TBM matrix of Eqn. 2 are obtained by taking the limit  $\rho, \sigma \rightarrow 0$ . These CP symmetries are therefore given as

$$X_1 = \frac{1}{3} \begin{pmatrix} 1 & -2 & 2 \\ -2 & -2 & -1 \\ 2 & -1 & -2 \end{pmatrix}, \quad X_2 = \frac{1}{3} \begin{pmatrix} -1 & 2 & -2 \\ 2 & -1 & -2 \\ -2 & -2 & -1 \end{pmatrix},$$

$$X_3 = \begin{pmatrix} -1 & 0 & 0 \\ 0 & 0 & 1 \\ 0 & 1 & 0 \end{pmatrix}, \quad X_4 = \begin{pmatrix} 1 & 0 & 0 \\ 0 & 1 & 0 \\ 0 & 0 & 1 \end{pmatrix}.$$

The residual flavor symmetries can be generated by the CP transformations as follows

$$\begin{aligned} G_1 &= X_2 X_3^* = X_3 X_2^* = X_4 X_1^* = X_1 X_4^*, \\ G_2 &= X_1 X_3^* = X_3 X_1^* = X_4 X_2^* = X_2 X_4^*, \\ G_3 &= X_1 X_2^* = X_2 X_1^* = X_4 X_3^* = X_3 X_4^*, \\ G_4 &= X_1 X_1^* = X_2 X_2^* = X_3 X_3^* = X_4 X_4^*. \end{aligned} \tag{15}$$

Notice that only three of the four CP and flavor symmetries are really independent. If any three of the four CP symmetries in Eqn. 14 are imposed simultaneously, the neutrino mixing matrix would reduce to the cTBM matrix in Eqn. 11 with  $\theta_{13} = 0$ . Therefore, we will impose only two or only one of these CP symmetries, so that realistic mixing patterns with non-vanishing  $\theta_{13}$  and CP violation are obtained.

The lepton mixing patterns, such as tribimaximal, golden ratio, and bi-maximal mixing, are excluded by current neutrino oscillation data, particularly by the precise measurement of the reactor angle,  $\theta_{13}$ . These patterns must be revamped to align with experimental results and to provide meaningful theoretical predictions for CP violation.

We assume neutrinos are Majorana particles and demonstrate how the application of residual flavor and CP symmetries can lead to systematic generalizations of the mixing patterns. By imposing these residual symmetries, we can determine the  $i$ -th column of the mixing matrix, thereby deriving generalized patterns that are both viable and predictive. Consequently, the mixing matrix can be characterized by a limited set of parameters.

### Case I : $G_1$ flavor and $X_1, X_4$ CP symmetries

As stated above, applying the generalized CP transformations represented by  $X_1$  and  $X_4$ , the neutrino mass matrix  $m_\nu$  transforms into its complex conjugate. The CP transformations  $X_1$  and  $X_4$  act as symmetries of  $m_\nu$ , which results in the preservation of the  $G_1$  flavor symmetry. Consequently, the neutrino mass matrix  $m_\nu$  must satisfy the symmetry constraints imposed by both the CP transformations  $X_1$  and  $X_4$  as

$$X_1^T m_\nu X_1 = m_\nu^*, \quad X_4^T m_\nu X_4 = m_\nu^*. \tag{16}$$

Therefore, the light neutrino mass matrix is of the following form

$$m'_\nu = U_{cTBM}^T m_\nu U_{cTBM} = \begin{pmatrix} m_1 & 0 & 0 \\ 0 & m_2 & \delta m \\ 0 & \delta m & m_3 \end{pmatrix}, \tag{17}$$

where the parameters  $m_1, m_2, m_3$  and  $\delta m$  are real. The mass matrix  $m'_\nu$  can be diagonalized by a real orthogonal matrix  $R_{23}(\theta)$  given by

$$R_{23}(\theta) = \begin{pmatrix} 1 & 0 & 0 \\ 0 & \cos \theta & \sin \theta \\ 0 & -\sin \theta & \cos \theta \end{pmatrix}, \quad \text{with } \tan 2\theta = \frac{2\delta m}{m_3 - m_2}. \tag{18}$$

As a result, in this case the lepton mixing matrix is given as

$$U = U_{cTBM} R_{23} Q_\nu, \tag{19}$$

such that

$$U = \frac{1}{\sqrt{6}} \begin{pmatrix} 2 & \sqrt{2}e^{-i\rho} \cos \theta & \sqrt{2}e^{-i\rho} \sin \theta \\ -e^{i\rho} & \sqrt{2} \cos \theta - \sqrt{3}e^{-i\sigma} \sin \theta & \sqrt{2} \sin \theta + \sqrt{3}e^{-i\sigma} \cos \theta \\ e^{i(\rho+\sigma)} & -\sqrt{3} \sin \theta - \sqrt{2}e^{i\sigma} \cos \theta & \sqrt{3} \cos \theta - \sqrt{2}e^{i\sigma} \sin \theta \end{pmatrix} Q_\nu. \quad (20)$$

Here  $Q_\nu = \text{diag}(e^{ik_1\pi/2}, e^{ik_2\pi/2}, e^{ik_3\pi/2})$  is a diagonal unitary matrix with  $k_{1,2,3} = 0, 1, 2, 3$  and  $\theta$  is the rotation angle. The entries  $\pm 1$  represents the CP parities of the neutrino states and ensure that the neutrino mass eigenvalues remain non-negative. One can notice that, the first column of the lepton mixing matrix in Eqn. 20

is given by  $\frac{1}{\sqrt{6}} \begin{pmatrix} 2 \\ -e^{i\rho} \\ e^{i(\rho+\sigma)} \end{pmatrix}$ . This column is consistent with that of the cTBM mixing pattern. It arises from the

preserved  $G_1$  symmetry. When other two CP symmetries  $X_2$  and  $X_3$  are imposed, the neutrino mass matrix also preserves the flavor symmetry  $G_1 = X_2 X_3^* = X_3 X_2^*$  as shown in Eqn 15. We can calculate the neutrino mixing angles from a given mixing matrix  $U$  by using the following relations

$$s_{12}^2 = \frac{|U_{12}|^2}{1 - |U_{13}|^2}, \quad s_{23}^2 = \frac{|U_{23}|^2}{1 - |U_{13}|^2}, \quad \text{and} \quad s_{13}^2 = |U_{13}|^2. \quad (21)$$

The Jarlskog rephasing invariant ( $J_{CP}$ ) is defined as

$$J_{CP} = \text{Im}(U_{11}U_{12}^*U_{21}U_{22}^*). \quad (22)$$

## Case II : $G_2$ flavor and $X_2, X_4$ CP symmetries

Accordingly, applying the generalized CP transformations represented by  $X_2$  and  $X_4$ , the neutrino mass matrix  $m_\nu$  transforms into its complex conjugate. The CP transformations  $X_2$  and  $X_4$  act as symmetries of  $m_\nu$ , which results in the preservation of the  $G_2$  flavor symmetry. Consequently, the neutrino mass matrix  $m_\nu$  must satisfy the symmetry constraints imposed by both the CP transformations  $X_2$  and  $X_4$  as

$$X_2^T m_\nu X_2 = m_\nu^*, \quad X_4^T m_\nu X_4 = m_\nu^*. \quad (23)$$

The light neutrino mass matrix will be

$$m'_\nu = U_{cTBM}^T m_\nu U_{cTBM} = \begin{pmatrix} m_1 & 0 & \delta m \\ 0 & m_2 & 0 \\ \delta m & 0 & m_3 \end{pmatrix}, \quad (24)$$

where the parameters  $m_1, m_2, m_3$  and  $\delta m$  are real. The mass matrix  $m'_\nu$  can be diagonalized by a real orthogonal matrix  $R_{13}(\theta)$  given by

$$R_{13}(\theta) = \begin{pmatrix} \cos \theta & 0 & \sin \theta \\ 0 & 1 & 0 \\ -\sin \theta & 0 & \cos \theta \end{pmatrix}, \quad \text{with} \quad \tan 2\theta = \frac{2\delta m}{m_3 - m_1}. \quad (25)$$

As a result, in this case the lepton mixing matrix is given as

$$U = U_{cTBM} R_{13} Q_\nu, \quad (26)$$

$$U = \frac{1}{\sqrt{6}} \begin{pmatrix} 2 \cos \theta & \sqrt{2}e^{-i\rho} & 2 \sin \theta \\ -e^{i\rho} \cos \theta - \sqrt{3}e^{-i\sigma} \sin \theta & \sqrt{2} & -e^{i\rho} \sin \theta + \sqrt{3}e^{-i\sigma} \cos \theta \\ e^{i(\rho+\sigma)} \cos \theta - \sqrt{3} \sin \theta & -\sqrt{2}e^{i\sigma} & e^{i(\rho+\sigma)} \sin \theta + \sqrt{3} \cos \theta \end{pmatrix} Q_\nu. \quad (27)$$

One can notice that the second column of the mixing matrix is given by  $\frac{1}{\sqrt{3}} \begin{pmatrix} e^{-i\rho} \\ 1 \\ -e^{i\sigma} \end{pmatrix}$ , which corresponds to the

cTBM mixing pattern. This correspondence arises due to the preserved  $G_2$  symmetry. When other two CP symmetries  $X_1$  and  $X_3$  are imposed, the neutrino mass matrix also preserves the flavor symmetry  $G_2 = X_1 X_3^* = X_3 X_1^*$  as shown in Eqn 15. The  $G_3$  symmetry is excluded from our analysis due to its prediction of a zero reactor mixing angle, which is experimentally disfavored.

### 3 Texture one zero with Generalized CP Symmetry

The neutrino mass matrix remains invariant under residual symmetries and is transformed into its complex conjugate when a generalized CP transformation is applied. By imposing one zero textures in the neutrino mass matrix, we obtain six distinct patterns that are consistent with current neutrino oscillation data. These six patterns can be simultaneously diagonalized according to the conditions outlined in Eqn. 26. Moreover, all six patterns satisfy the generalized CP conditions specified in Eqn. 16 and 23. Here, we will explore the one zero textures within the framework of generalized CP symmetries

$$\begin{aligned}
 m_I &= \begin{pmatrix} 0 & \times & \times \\ \times & \times & \times \\ \times & \times & \times \end{pmatrix}, & m_{II} &= \begin{pmatrix} \times & 0 & \times \\ 0 & \times & \times \\ \times & \times & \times \end{pmatrix}, \\
 m_{III} &= \begin{pmatrix} \times & \times & 0 \\ \times & \times & \times \\ 0 & \times & \times \end{pmatrix}, & m_{IV} &= \begin{pmatrix} \times & \times & \times \\ \times & 0 & \times \\ \times & \times & \times \end{pmatrix}, \\
 m_V &= \begin{pmatrix} \times & \times & \times \\ \times & \times & 0 \\ \times & 0 & \times \end{pmatrix}, & m_{VI} &= \begin{pmatrix} \times & \times & \times \\ \times & \times & \times \\ \times & \times & 0 \end{pmatrix}.
 \end{aligned}$$

The presence of one zero textures in the neutrino mass matrix leads to a complex equation, which is given as

$$m_1 A + m_2 B + m_3 C = 0, \quad (28)$$

where  $A = U_{a1}U_{b1}$ ,  $B = U_{a2}U_{b2}$ ,  $C = U_{a3}U_{b3}$  and  $U_{a1}, U_{b1}, U_{a2}, U_{b2}, U_{a3}, U_{b3}$  are the elements of mixing matrix. The above complex equation yields two mass ratios

$$\frac{m_1}{m_2} = \frac{\text{Re}(C)\text{Im}(B) - \text{Re}(B)\text{Im}(C)}{\text{Re}(A)\text{Im}(C) - \text{Re}(C)\text{Im}(A)}, \quad (33)$$

and

$$\frac{m_1}{m_3} = \frac{\text{Re}(C)\text{Im}(B) - \text{Re}(B)\text{Im}(C)}{\text{Re}(B)\text{Im}(A) - \text{Re}(A)\text{Im}(B)}. \quad (29)$$

Where Re (Im) denotes the real (imaginary) part. These mass ratios can be used to obtain the expression for the parameter  $R_\nu$ , which is the ratio of mass squared differences ( $\Delta m_{ij}^2 = m_i^2 - m_j^2$ ),

$$R_\nu \equiv \frac{\Delta m_{21}^2}{|\Delta m_{31}^2|} = \frac{\left(\frac{m_2}{m_1}\right)^2 - 1}{\left|\left(\frac{m_3}{m_1}\right)^2 - 1\right|}. \quad (30)$$

Here  $m_1 > m_3$  for an inverted mass hierarchy (IH) and  $m_1 < m_3$  for the normal mass hierarchy (NH).

### 4 Results and Discussions

The neutrino mass matrix is constructed using the mixing matrix given in Eqn. 20 and 27, and subjected to generalized CP conditions derived from Eqn. 13. We observed that all neutrino mass matrices with one zero textures are consistent with these generalized CP conditions, i.e., with  $X_1$  and  $X_2$ . In the analysis, we have sampled  $10^8$  points to scan the complete parameter space and used the mass squared differences  $\Delta m_{\text{solar}}^2$  and  $\Delta m_{\text{atm}}^2$ , varying them within their  $3\sigma$  ranges, as indicated in Table 1. The rotation angle  $\theta$  varied from 0 to  $\frac{\pi}{2}$ . Additionally, the Majorana phases ( $\rho$  and  $\sigma$ ) are explored freely over their entire permissible ranges i.e., from  $(0 - 2\pi)$ . The one zero textures constraint is applied by the parameter  $R_\nu$ , representing mass ratios, which are allowed to lie within the  $3\sigma$  range according to Eqn. 30. For each of the six texture one zero patterns, we computed the possible values of the effective Majorana mass for both normal hierarchy (NH) and inverted hierarchy (IH) with  $X_1$  and  $X_2$  respectively, as detailed in Tables 2 and 3. To assess the compatibility of the effective Majorana mass ( $m_{ee}$ ), we incorporated constraints from the KamLAND-Zen [42, 43], LEGEND [44], CUORE [45], and nEXO experiments [46], which are represented by the horizontal lines in the figures. For the lightest neutrino mass ( $m_{\text{lightest}}$ ), we considered the experimental bounds set by the Karlsruhe Tritium Neutrino

Experiment (KATRIN). We have used the KATRIN limit, i.e., 0.8 eV, and KATRIN’s proposed sensitivity, i.e., 0.2 eV [47]. To enhance the predictability of our model, we have also used the proposed sensitivity by the Project 8 experiment, which aims for a sensitivity around 40 meV, is shown as vertical lines in the figures where  $m_{ee}$  is plotted against the lightest neutrino mass. The cosmological limit on the sum of neutrino masses,  $\Sigma m_i < 0.12$  eV, provided by the Planck data [48], is shown as vertical lines in the figures where  $m_{ee}$  is plotted against the sum of neutrino masses. The DESI experiment proposed a very stringent bound on sum of neutrino mass, i.e., 0.072eV. We also adopted the upper bound of  $\sum m_\nu < 0.17$  eV, obtained from the combination of the P20<sub>H</sub>+DESI/SDSS+DES-SN datasets in the  $\Lambda$ CDM + Fluid DR +  $\sum m_\nu$  model at 95% confidence level which provides the relaxation on Planck data [49].

## Analysis of $X_1$ Condition

For the  $X_1$  condition, we obtained values for the  $m_{ee}$  as a function of the lightest neutrino mass constrained by the  $R_\nu$  parameter at  $3\sigma$  range, which are consistent with current and future experimental data, as detailed in Table 2.

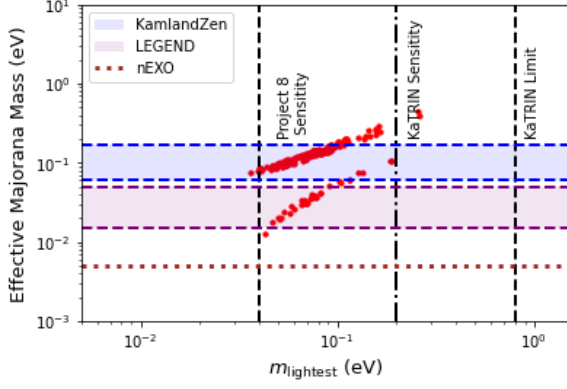
S.No.	Textures	Hierarchy	Effective Majorana mass(eV)	Lightest Neutrino mass(eV)	Sum of mass(eV)
1	$m_I$	Normal	0.0	0.0019-0.0080	0.042-0.073
		Inverted	-	-	-
2	$m_{II}$	Normal	0.016-0.52	0.036-0.33	0.14-1.38
		Inverted	0.050-0.72	0.047-0.42	0.22-1.17
3	$m_{III}$	Normal	0.011-0.51	0.036-0.28	0.14-0.89
		Inverted	0.013-0.27	0.065-0.44	0.18-0.70
4	$m_{IV}$	Normal	0.0009-0.49	0.0093-0.28	0.073- 2.53
		Inverted	0.052-0.42	0.049-0.27	0.18-0.93
5	$m_V$	Normal	0.028-0.57	0.049-0.33	0.16-0.84
		Inverted	0.058-0.15	0.061-0.26	0.21-0.86
6	$m_{VI}$	Normal	0.0009-0.44	0.0097-0.21	0.073-1.45
		Inverted	0.052-0.25	0.052-0.39	0.19-1.17

Table 2: Values of the effective Majorana mass, lightest neutrino mass, and the sum of the three neutrino masses for both NH and IH for the  $X_1$  condition.

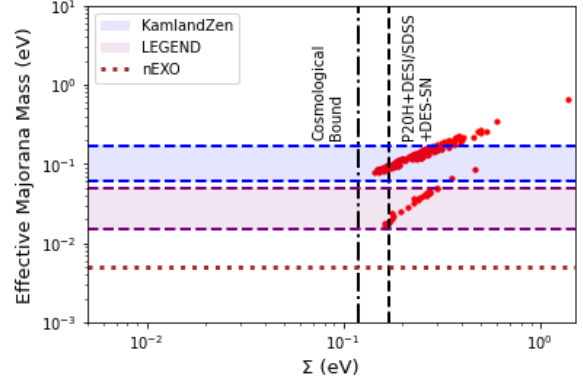
The cosmological bound on the sum of neutrino masses,  $\Sigma m_i < 0.12$  eV, excludes compatibility for the mass matrices  $m_{II}$ ,  $m_{III}$ , and  $m_V$  in NH. The inverted hierarchy (IH) is excluded from the analysis because all one zero texture matrices in the IH are inconsistent with Planck data and P20<sub>H</sub> + DESI/SDSS + DES-SN datasets, within the  $\Lambda$ CDM + Fluid DR +  $\sum m_\nu$  model at the 95% confidence level. In other words, matrices with one zero in the diagonal positions remain consistent with the cosmological bound in NH. The detailed description of the textures is given below:

- I. The mass matrix  $m_I$ , which has a zero in the (1,1) position, cannot support inverted hierarchy because it predicts a large value for the reactor mixing angle ( $\theta_{13}$ ), which is experimentally disfavored. The imposition of generalized CP conditions does not change this property. For NH, the effective Majorana mass also vanishes.
- II. Figure 1a depicts the correlation between the  $m_{ee}$  and  $m_{\text{lightest}}$  for the mass matrix  $m_{II}$  in NH, characterized by a zero texture at the (1,2) position. The analysis reveals that this matrix is consistent with both current and future experimental constraints. The lower bound on  $m_{ee} \leq 0.016$  eV is within the sensitivity reach of KamLAND-Zen, LEGEND, and nEXO experiment. The lightest neutrino mass shows the compatibility with the proposed sensitivities of KATRIN and Project 8 experiment. Figure 1b illustrates the correlation between the  $m_{ee}$  and the sum of neutrino masses( $\Sigma m_i$ ). The results indicate compatibility with the P20H+DESI/SDSS+DES-SN dataset,  $\Sigma m_i < 0.17$  eV, but incompatible with the Planck limit.



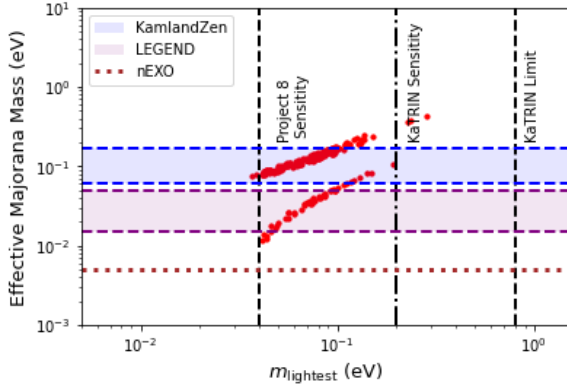


(a)

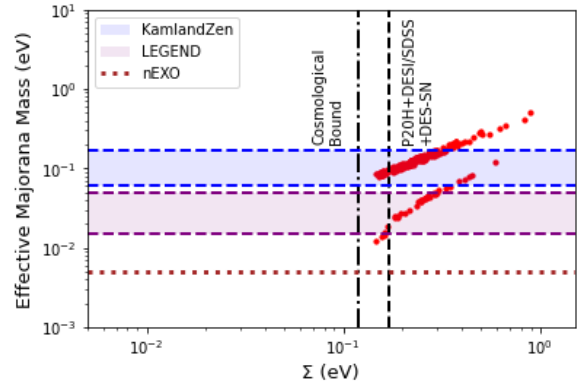


(b)

Figure 1: Effective Majorana mass with respect to lightest neutrino mass(left) and sum of neutrino mass(right) for mass matrix  $m_{II}$  in NH for  $X_1$ .

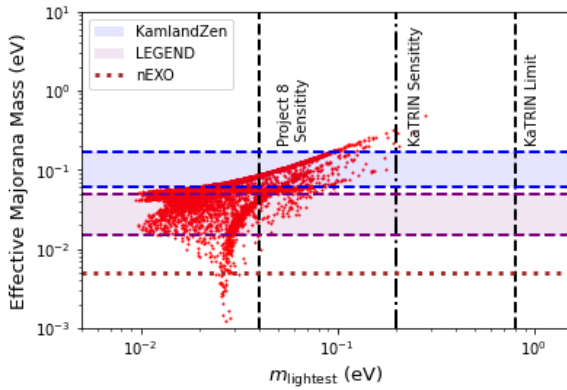


(a)

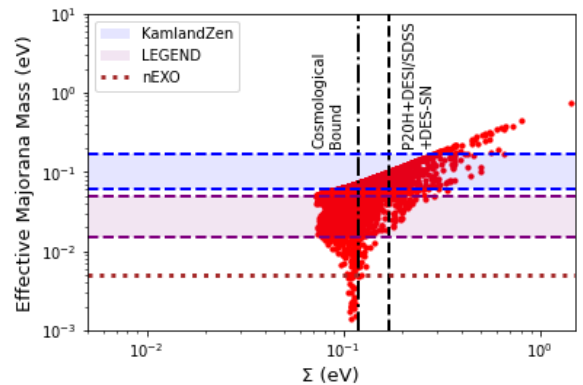


(b)

Figure 2: Effective Majorana mass with respect to lightest neutrino mass(left) and sum of neutrino mass(right) for mass matrix  $m_{III}$  in NH for  $X_1$ .



(a)



(b)

Figure 3: Effective Majorana mass with respect to lightest neutrino mass(left) and sum of neutrino mass(right) for mass matrix  $m_{IV}$  in NH for  $X_1$ .

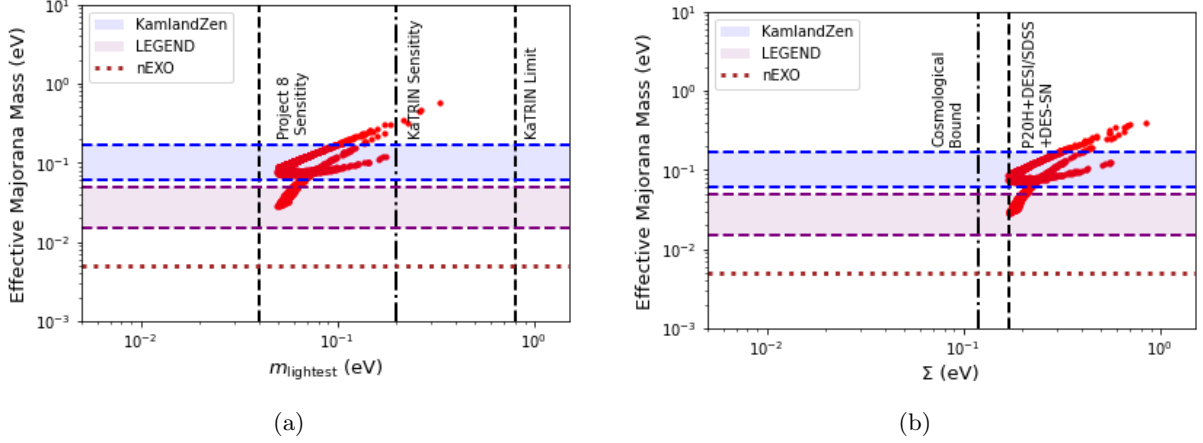


Figure 4: Effective Majorana mass with respect to lightest neutrino mass(left) and sum of neutrino mass(right) for mass matrix  $m_V$  in NH for  $X_1$ .

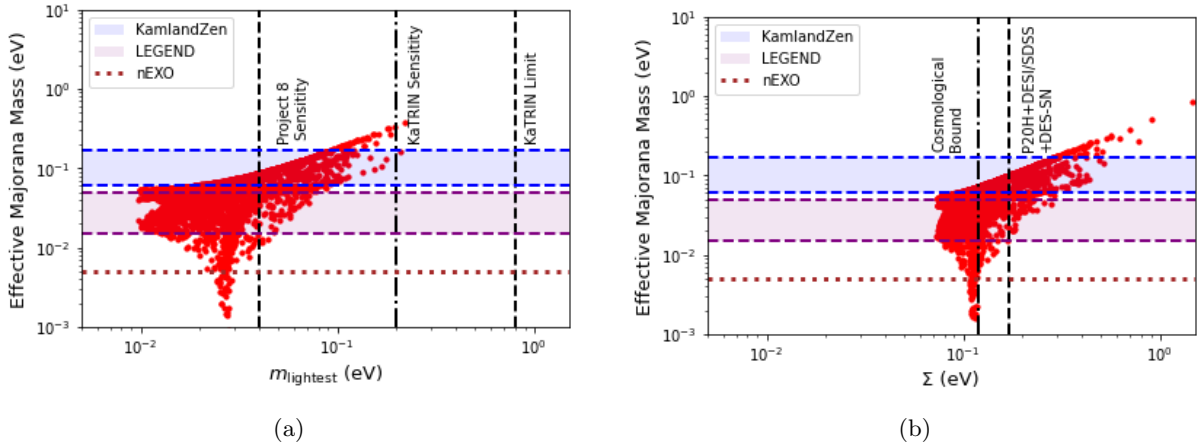


Figure 5: Effective Majorana mass with respect to lightest neutrino mass(left) and sum of neutrino mass(right) for mass matrix  $m_{V_I}$  in NH for  $X_1$ .

- III. Figure 2a illustrates the correlation between  $m_{ee}$  and  $m_{\text{lightest}}$  for the mass matrix  $m_{III}$  in NH, having zero at (1,3) position. The analysis confirms that this matrix is consistent with both current experimental constraints and proposed sensitivities of KATRIN and Project 8, on  $m_{\text{lightest}}$ . The lower bound on  $m_{ee} \leq 0.011$  eV is within the sensitivity reach of KamLAND-Zen, LEGEND, and nEXO. Figure 2b depicts the correlation between  $m_{ee}$  and  $\Sigma m_i$ . The results indicate compatibility with the P20H+DESI/SDSS+DES-SN dataset, which constrains  $\Sigma m_i < 0.17$  eV, but show incompatibility with the Planck limit.
- IV. Figure 3a shows the correlation between the  $m_{ee}$  and  $m_{\text{lightest}}$  for the mass matrix  $m_{IV}$  in the normal hierarchy (NH), with a zero at (2,2) position. The analysis demonstrates that this matrix is consistent with both current and future experimental constraints. The lower bound on  $m_{ee} \leq 0.0009$  eV is within the sensitivity reach of KamLAND-Zen, LEGEND, and nEXO. The lightest neutrino mass is compatible with the proposed sensitivities of the KATRIN and Project 8 experiments. Figure 3b presents the correlation between  $m_{ee}$  and  $\Sigma m_i$ . The results show that the matrix is compatible with both the P20H+DESI/SDSS+DES-SN dataset and the Planck limit.
- V. Figure 4a depicts the correlation between the  $m_{ee}$  and  $m_{\text{lightest}}$  for the mass matrix  $m_V$  in NH, characterized by texture zero at the (2,3) position. The analysis reveals that this matrix is consistent with both current and future experimental constraints. The lower bound on  $m_{ee} \leq 0.028$  eV

is within the sensitivity reach of KamLAND-Zen, LEGEND experiment. Figure 4b illustrates the correlation between the  $m_{ee}$  and  $\Sigma m_i$ . The results indicate incompatibility with the cosmological bound but compatible with the P20H+DESI/SDSS+DES-SN dataset.

- VI. Figure 5a shows the correlation between the  $m_{ee}$  and  $m_{\text{lightest}}$  for the mass matrix  $m_{VI}$  in NH, characterized by a texture zero at the (3,3) position. The analysis reveals that this matrix is consistent with both current and future experimental constraints. The effective Majorana mass spans the range (0.0009 - 0.44)eV, sensitive to all the considered experimental range. The lightest neutrino mass shows compatibility with the proposed limits of KATRIN and Project 8 experiment. Figure 5b illustrates the correlation between the  $m_{ee}$  and  $\Sigma m_i$ . The results indicate compatibility with the cosmological bound as well as with the P20H+DESI/SDSS+DES-SN dataset on the sum of neutrino masses. The sum of neutrino masses is confined to the range (0.073 - 1.45)eV.

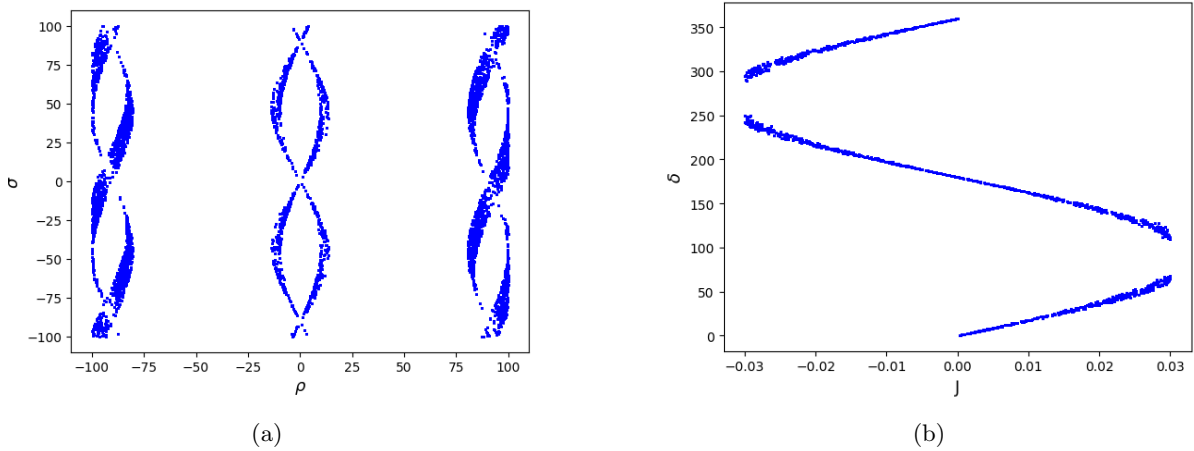


Figure 6: Correlation between Majorana phases  $\sigma$  and  $\rho$ (left) and Jarsklog Invariant  $J$  and  $\delta$ (right) for mass matrix  $m_{IV}$  in NH for  $X_1$ .

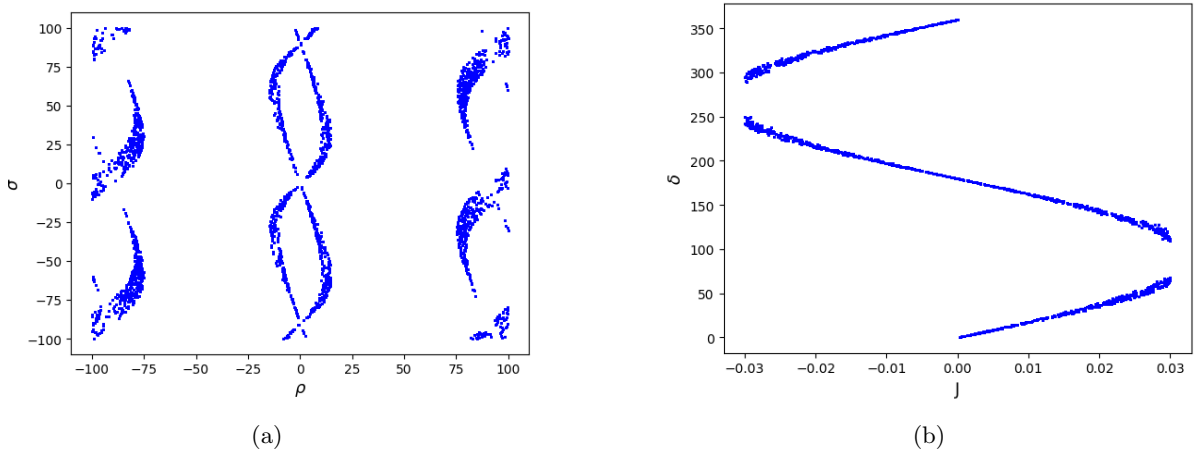


Figure 7: Correlation between Majorana phases  $\sigma$  and  $\rho$ (left) and Jarsklog Invariant  $J$  and  $\delta$ (right) for mass matrix  $m_{VI}$  in NH for  $X_1$ .

We have presented the correlation plots of various parameters for matrices  $m_{IV}$  and  $m_{VI}$ , as only they are compatible with the Planck data as well as with P20H+DESI/SDSS+DES-SN dataset. Figure 6a, shows the correlation between the two Majorana phases  $\rho$  and  $\sigma$ , and indicates that  $\rho$  is sharply constrained around 0 and  $\pm\pi/2$  for matrix  $m_{IV}$ . Figure 6b shows the correlation between Jarsklog invariant( $J$ ) and Dirac CP phase( $\delta$ ) for matrix  $m_{IV}$ , which shows the allowed parameter space. Figure 7a also shows the correlation between the

two Majorana phases  $\rho$  and  $\sigma$ , and indicates that  $\rho$  is sharply constrained around 0 and  $\pm\pi/2$  for matrix  $m_{VI}$ . Figure 7b shows the correlation between Jarlskog invariant and Dirac CP phase for matrix  $m_{VI}$ .

The Figure 8a shows a correlation between two mixing angles,  $\theta_{12}$  and  $\theta_{23}$ , constrained the allowed parameter space,  $35.03^\circ < \theta_{12} < 35.27^\circ$  with respect to the  $3\sigma$  range of  $\theta_{23}$  for mass matrix  $m_{IV}$ . Figure 8b shows allowed parameter space for J and  $\theta$  for mass matrix  $m_{VI}$ . Figure 9a shows the correlation between the  $\theta_{23}$  and  $\theta$ , indicates two allowed values for rotation mixing angle within the region  $0^\circ \leq \theta \leq 11.1^\circ$  and  $81.1^\circ \leq \theta \leq 88.8^\circ$  with  $3\sigma$  range of  $\theta_{23}$  for mass matrix  $m_{IV}$ . Figure 9b shows the correlation between the  $\theta_{13}$  and  $\theta$  for mass matrix  $m_{VI}$ . It is observed that for the  $X_1$  condition,  $\theta$  is tightly constrained to the range 14.30 - 15.60 degrees corresponding to the  $3\sigma$  allowed range of  $\theta_{13}$ . Figure 10a shows the allowed parameter space for J with mixing angle  $\theta_{23}$  for mass matrix  $m_{IV}$ . Figure 10b shows the allowed parameter space for  $\theta$  with  $3\sigma$  range of  $\theta_{12}$  for mass matrix  $m_{VI}$ .

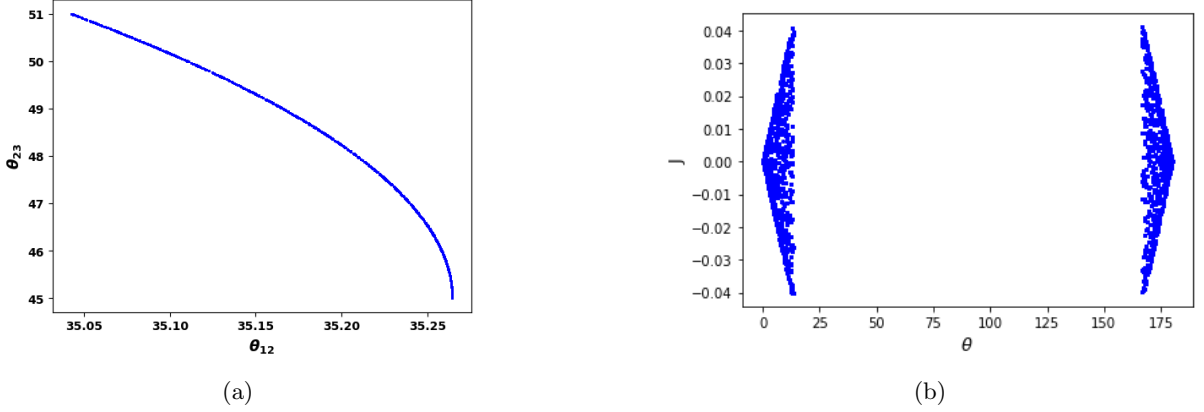


Figure 8: Correlation between mixing angle  $\theta_{23}$  and  $\theta_{12}$  for matrix  $m_{IV}$  in NH(left) and J and rotation angle  $\theta$  for matrix  $m_{VI}$  in NH(right) for  $X_1$  condition.

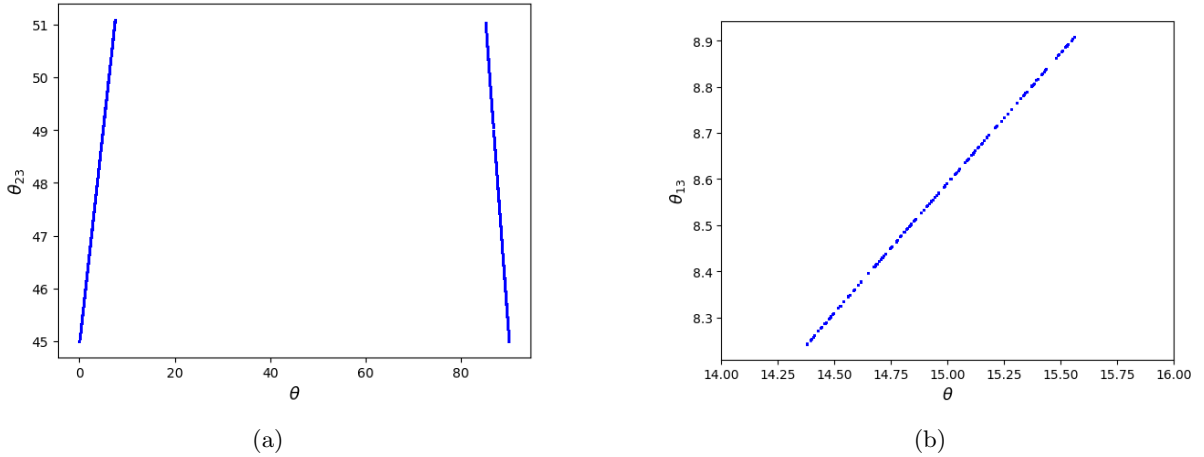


Figure 9: Correlation between mixing angle  $\theta_{23}$  and  $\theta$  for matrix  $m_{IV}$  in NH(left) and  $\theta_{13}$  and rotation angle  $\theta$  for matrix  $m_{VI}$  in NH(right) for  $X_1$  condition.

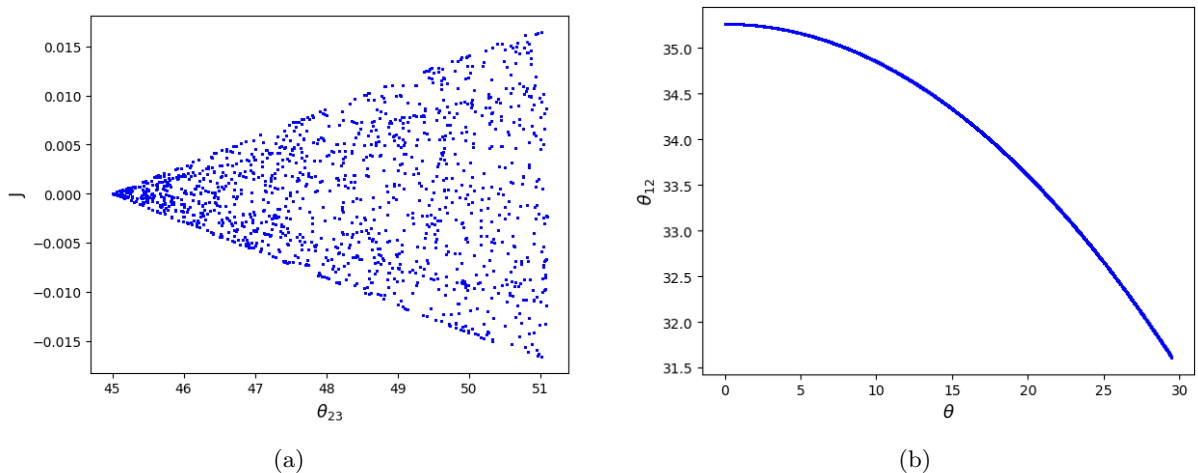


Figure 10: Correlation between Jarsklog Invariant  $J$  and mixing angle  $\theta_{23}$  for matrix  $m_{IV}$  in NH(left) and  $\theta_{12}$  and rotation angle  $\theta$  for matrix  $m_{VI}$  in NH(right) for  $X_1$  condition.

### Analysis of $X_2$ Condition

Similarly for the  $X_2$  condition, we have derived  $m_{ee}$  as a function of the lightest neutrino mass, constrained by the  $R_\nu$  parameter within the  $3\sigma$  range, aligns with both current and future experimental data as shown in Table 3.

S.No.	Textures	Hierarchy	Effective Majorana mass(eV)	Lightest Neutrino mass(eV)	Sum of mass(eV)
1	$m_I$	Normal	0.0	0.0021-0.0077	0.054-0.071
		Inverted	-	-	-
2	$m_{II}$	Normal	0.00055-0.16	0.0034-0.11	0.062-0.25
		Inverted	0.023-1.34	0.056-0.88	0.20-1.37
3	$m_{III}$	Normal	0.017-0.54	0.027-0.34	0.013-1.55
		Inverted	0.048-0.21	0.010-0.15	0.18-0.75
4	$m_{IV}$	Normal	0.023-0.52	0.036-0.30	0.13-1.25
		Inverted	0.016-0.48	0.048-0.27	0.18-0.40
5	$m_V$	Normal	0.047-0.41	0.0016-0.24	0.12-0.77
		Inverted	0.061-0.26	0.058-0.15	0.21-0.86
6	$m_{VI}$	Normal	0.024-0.28	0.026-0.16	0.13-1.05
		Inverted	0.051-0.40	0.049-0.22	0.18-1.17

Table 3: Values of the effective Majorana mass, lightest neutrino mass, and the sum of the three neutrino masses for both NH and IH for the  $X_2$  condition.

The cosmological upper limit on the sum of neutrino masses,  $\Sigma m_i < 0.12$  eV, excludes the mass matrices  $m_{IV}$ ,  $m_V$  and  $m_{VI}$  from compatibility. The inverted hierarchy (IH) is excluded from the analysis because all one zero texture matrices in the IH are inconsistent with Planck data and P20<sub>H</sub> + DESI/SDSS + DES-SN datasets, within the  $\Lambda$ CDM + *Fluid DR* +  $\Sigma m_\nu$  model at the 95% confidence level. The detailed description of textures is given below:

- I. The mass matrix  $m_I$ , characterized by a zero in the (1,1) position, cannot support inverted hierarchy because it predicts a large value for the reactor mixing angle ( $\theta_{13}$ ), which is experimentally not allowed. The imposition of generalized CP conditions does not change this property. For NH, the effective Majorana mass also vanishes.
- II. Figure 11a depicts the correlation between the  $m_{ee}$  and  $m_{\text{lightest}}$  for the mass matrix  $m_{II}$  in NH, characterized by a texture zero at the (1,2) position. The analysis reveals that this matrix is consistent with both current and future experimental constraints. The effective Majorana mass spans the range (0.0005

- 0.16)eV, while the lightest neutrino mass varies within (0.0034 - 0.11)eV. Figure 11b illustrates the correlation between the effective Majorana mass and the sum of neutrino masses  $\Sigma m_i$ . The results indicate compatibility with the cosmological bound on the sum of neutrino masses,  $\Sigma m_i < 0.12$  eV, established by Planck data as well as DESI/SDSS+Pantheon+DES-SN dataset. The sum of neutrino masses is confined to the range (0.062 - 0.25)eV.

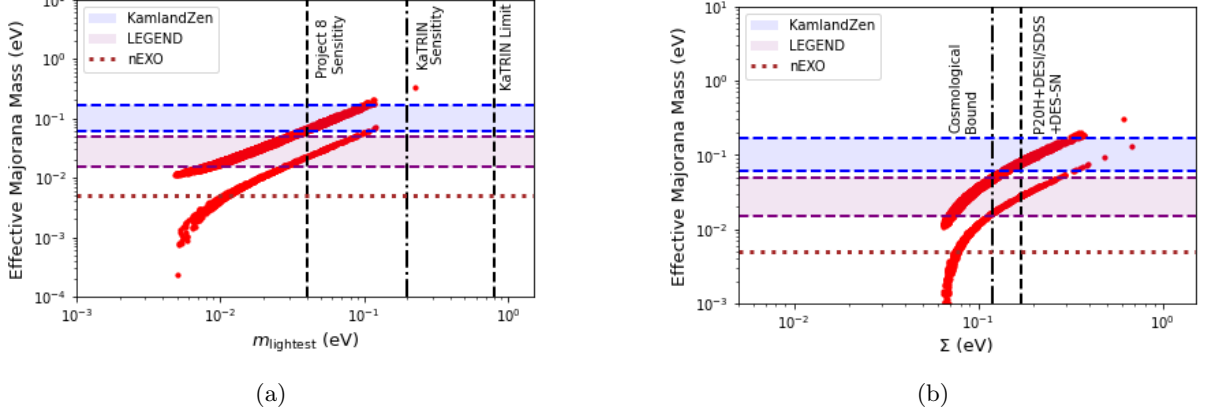


Figure 11: Effective Majorana mass with respect to lightest Neutrino mass(left) and sum of neutrino mass(right) for mass matrix  $m_{II}$  in NH for  $X_2$ .

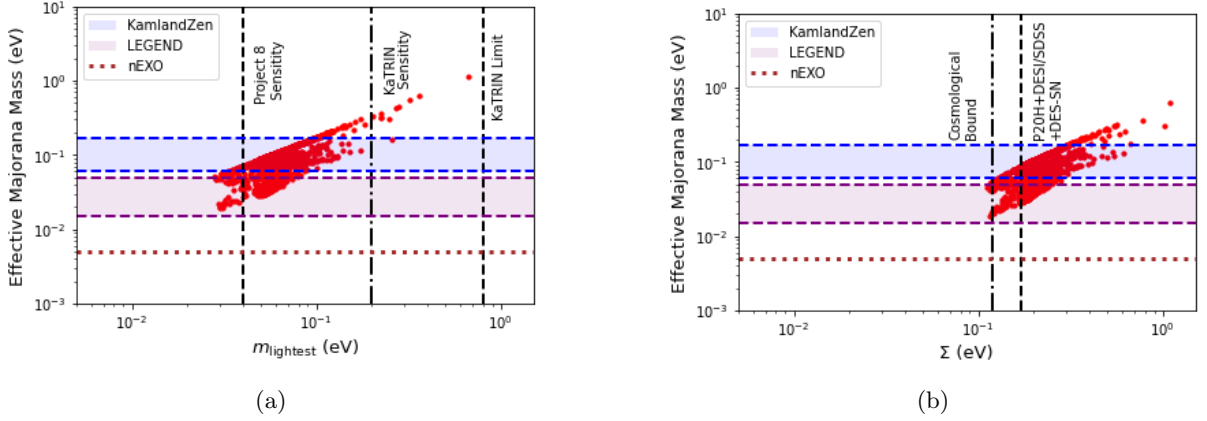
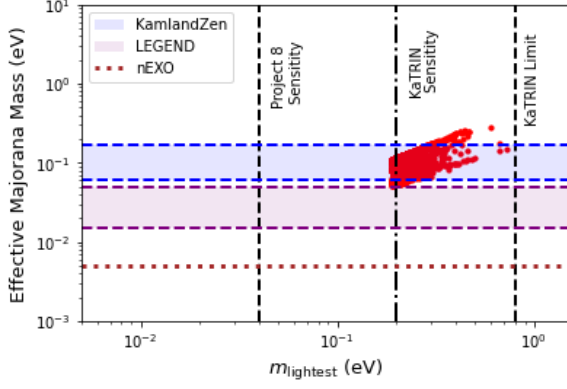


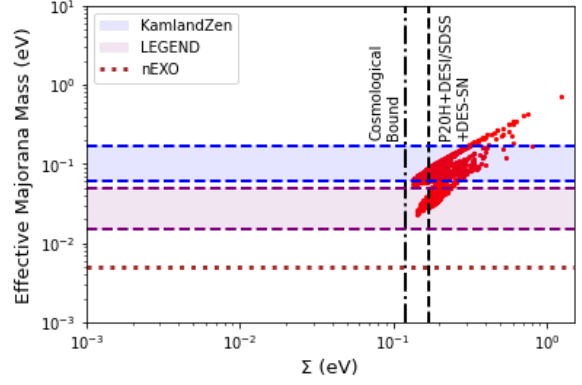
Figure 12: Effective Majorana mass with respect to lightest neutrino mass(left) and sum of neutrino mass(right) for mass matrix  $m_{III}$  in NH for  $X_2$ .

III. Figure 12a shows the correlation between the  $m_{ee}$  and  $m_{\text{lightest}}$  for the mass matrix  $m_{III}$ , with a zero at the (1,3) position. The analysis shows that this matrix is consistent with both current and future experimental constraints. The effective Majorana mass spans the range (0.024 - 0.25)eV, while the lightest neutrino mass lies within (0.039 - 0.16)eV. Figure 12b illustrates the correlation between the effective Majorana mass and  $\Sigma m_i$ . The results indicate compatibility with the cosmological bound as well as DESI/SDSS+Pantheon+DES-SN dataset. The sum of neutrino masses is confined to the range (0.13 - 1.55)eV.

IV. Figure 13a illustrates the correlation between the  $m_{ee}$  and  $m_{\text{lightest}}$  for the mass matrix  $m_{IV}$ , with a zero at the (2,2) position. The analysis shows that,  $m_{ee}$  have lower bound at 0.023eV, shows compatibility with the KamLANDZEN and LEGEND experiments. The  $m_{\text{lightest}}$  are in the detectable range of KaTRIN experiment. Figure 13b shows the correlation between the effective Majorana mass and  $\Sigma m_i$ . The results indicate incompatibility with the cosmological bound but compatible with the DESI/SDSS+Pantheon+DES-SN dataset. The sum of neutrino masses is confined to the range (0.13-1.25)eV.

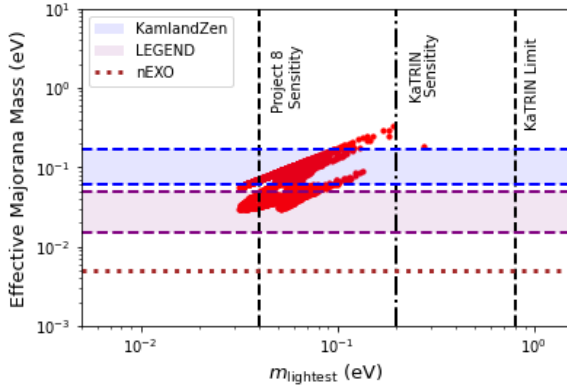


(a)

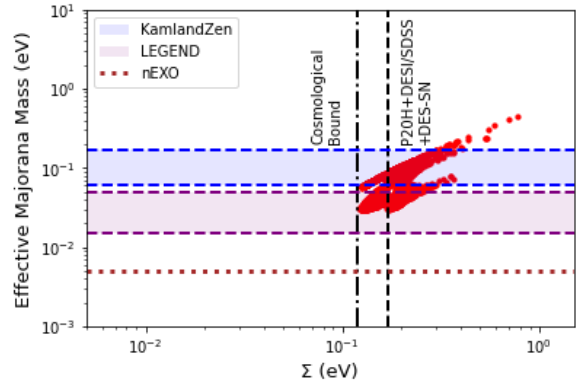


(b)

Figure 13: Effective Majorana mass with respect to lightest neutrino mass(left) and sum of neutrino mass(right) for mass matrix  $m_{IV}$  in NH for  $X_2$ .

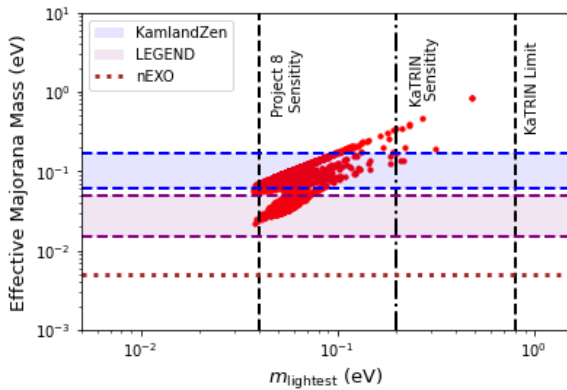


(a)

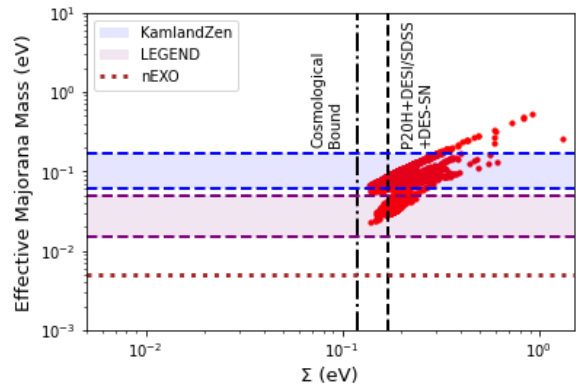


(b)

Figure 14: Effective Majorana mass with respect to lightest neutrino mass(left) and sum of neutrino mass(right) for mass matrix  $m_V$  in NH for  $X_2$ .



(a)



(b)

Figure 15: Effective Majorana mass with respect to lightest neutrino mass(left) and sum of neutrino mass(right) for mass matrix  $m_{VI}$  in NH for  $X_2$ .

V. Figure 14a depicts the correlation between the  $m_{ee}$  and  $m_{\text{lightest}}$  for the mass matrix  $m_V$ , having zero at the (2,3) position. The analysis provides lower bound on  $m_{ee}$ , shows compatibility with the KamLAND

Zen and LEGEND experiment. The  $m_{\text{lightest}}$  is compatible with the proposed sensitivities of KATRIN and project 8 experiment. Figure 14b illustrates the correlation between the  $m_{ee}$  and  $\Sigma m_i$ . The results indicate compatibility with the cosmological bound as well as DESI/SDSS+Pantheon+DES-SN dataset. The sum of neutrino masses is confined to the range (0.12-0.77)eV.

VI. Figure 15a shows the correlation between the  $m_{ee}$  and the  $m_{\text{lightest}}$  for the mass matrix  $m_{VI}$ , characterized by a zero at the (3,3) position. The analysis shows that this matrix is consistent with current experimental constraints. The effective Majorana mass spans the range (0.024 - 0.25)eV, while the lightest neutrino mass lies within (0.039 - 0.16)eV. Figure 15b depicts the correlation between the  $m_{ee}$  and the  $\Sigma m_i$ . The results indicate incompatibility with the cosmological bound but compatible with the DESI/SDSS+Pantheon+DES-SN dataset. The sum of neutrino masses is confined to the range (0.13 - 1.55)eV.

The Figure 16a and 16b shows the allowed parameter space for matrices  $m_{II}$  and  $m_{III}$ , respectively, which indicates that  $\rho$  is sharply constrained in the region around  $\rho = 0, \frac{\pi}{2}, \pi, \frac{3\pi}{2}, 2\pi$ . The different mixing matrix, as shown in Eqn. 20 and 27, predicts specific correlations between the mixing angle  $\theta_{23}$  and the CP-violating phase  $\delta$  when one zero textures are introduced. As  $\theta_{23}$  tends towards maximal mixing, the corresponding CP violation is also expected to reach maximality, with  $\delta$  approaching values of  $\pi/2$  or  $3\pi/2$  shown in Figure 17a and 17b.

We also demonstrate correlation between the mixing angles  $\theta_{12}$ ,  $\theta_{23}$ , and the free parameter  $\theta$ . Moreover, in all neutrino mass matrices featuring one zero textures with or without additional symmetries a complementary relationship emerges between the predicted values of  $\theta_{23}$  and  $\delta$  for specific patterns. For instance, the pattern  $m_{12} = 0$  is complementary to  $m_{13} = 0$ , and similarly,  $m_{22} = 0$  complements  $m_{33} = 0$ .

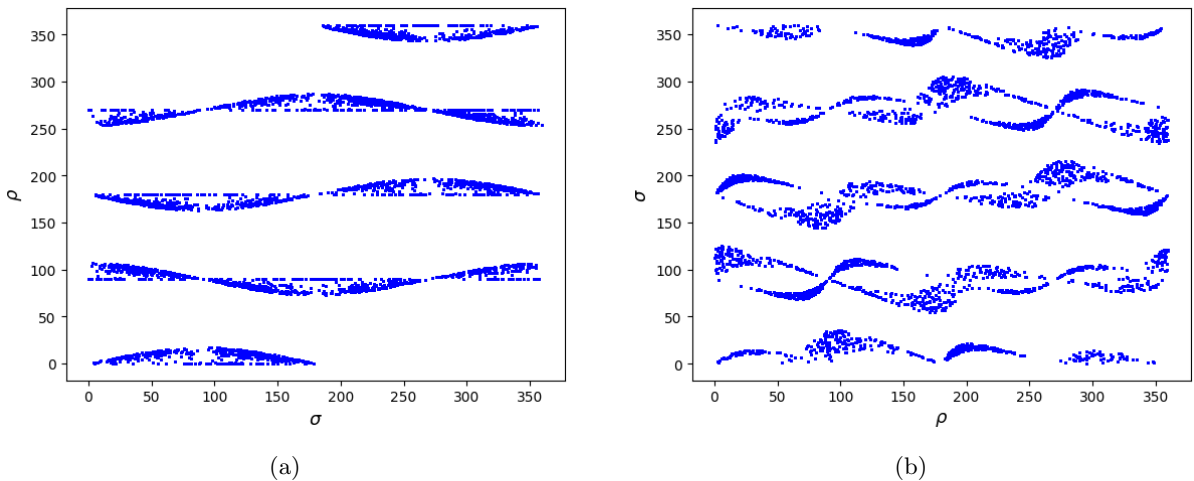


Figure 16: Correlation between Majorana phases  $\sigma$  and  $\rho$  for mass matrix  $m_{II}$  in NH(left) and Majorana phases  $\sigma$  and  $\rho$  for mass matrix  $m_{III}$  in NH(right) for  $X_2$ .

This complementarity arises from the transformation of  $m_{12}$  (or  $m_{22}$ ) into  $m_{13}$  (or  $m_{33}$ ) via the exchange

$$\theta_{23} \rightarrow \frac{\pi}{2} - \theta_{23}, \quad \delta \rightarrow \pi + \delta.$$

Thus, the predictions for  $\theta_{23}$  in the case  $m_{12} = 0$  ( $m_{33} = 0$ ) reflect those for  $m_{13} = 0$  ( $m_{22} = 0$ ) around  $\theta_{23} = \frac{\pi}{4}$ . Similarly, the prediction for  $\delta$  in the case  $m_{13} = 0$  ( $m_{33} = 0$ ) is related to the corresponding prediction for  $m_{12} = 0$  ( $m_{22} = 0$ ) by a constant phase shift of  $\pi$ .

Figure 18a depicts allowed parameter space for J with respect to the rotation angle  $\theta$  for mass matrix  $m_{II}$ . The correlation between the mixing angles  $\theta_{12}$  and  $\theta_{23}$  for mass matrix  $m_{III}$ , shown in Figure 18b, indicates the highly constrained region for  $\theta_{12}$  with respect to the allowed  $3\sigma$  range of  $\theta_{23}$ . The allowed region for  $\theta$  with respect to  $3\sigma$  ranges of the mixing angles  $\theta_{13}$  and  $\theta_{23}$  are presented in the Figures 19a and 19b for mass matrix  $m_{III}$ . The Figure 20a shows the allowed parameter space for  $m_{\text{lightest}}$  and  $\delta$  for mass matrix  $m_{II}$ . The Figure 20b shows the allowed region of parameter J with respect to the mixing angle  $\theta_{23}$  for mass matrix  $m_{II}$ . The correlation between  $\theta$  and  $\theta_{12}$  for mass matrix  $m_{II}$ , is shown in 21a. The allowed parameter space for J with respect to  $\theta_{12}$  for mass matrix  $m_{III}$ , is shown in 21b.



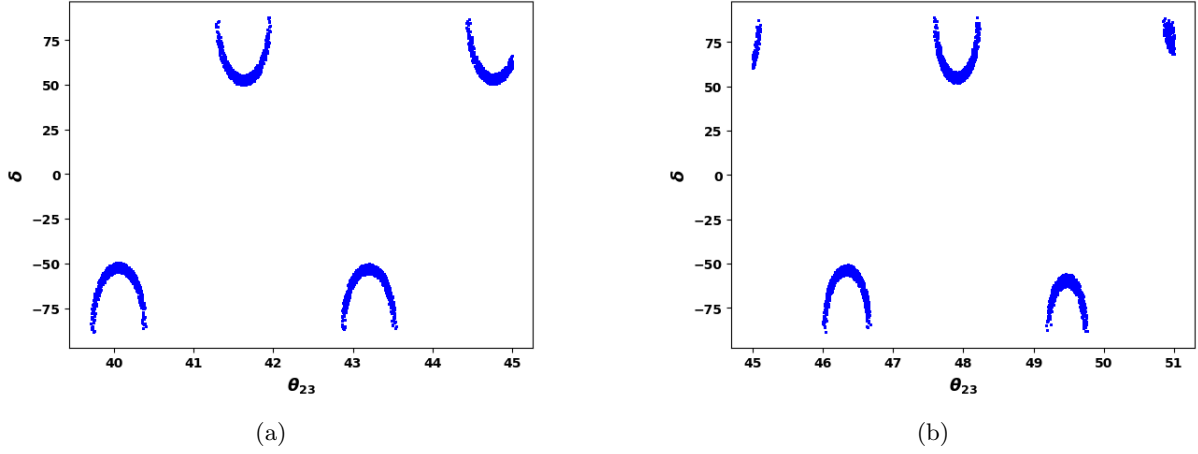


Figure 17: Correlation between mixing angle  $\theta_{23}$  and  $\delta$  for matrix  $m_{IV}$  in NH for  $X_1$  condition(left) and  $J$  and  $\delta$  for matrix  $m_{II}$  in NH(right) for  $X_2$  condition.

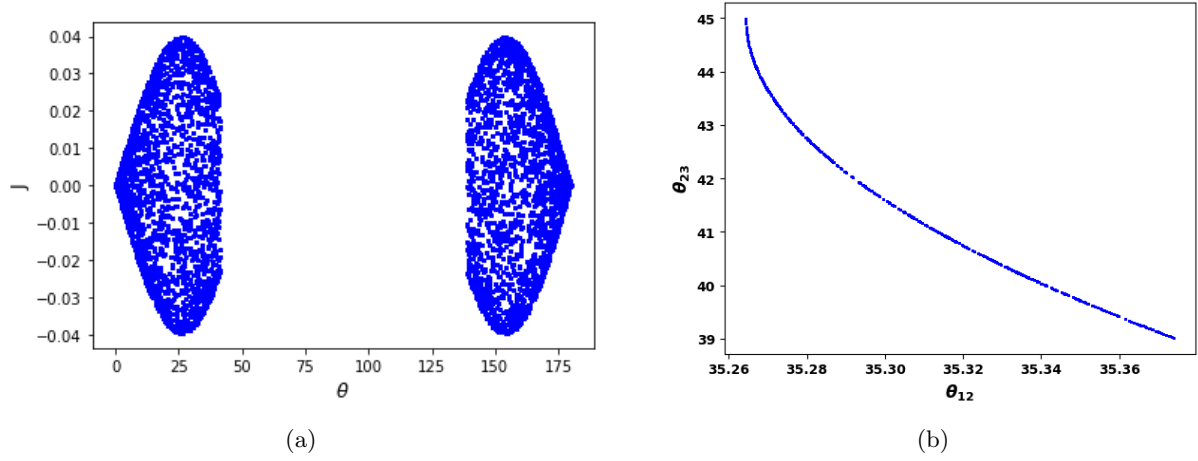


Figure 18: Correlation between rotation angle  $\theta$  and  $J$  for matrix  $m_{II}$  in NH(left) and  $\theta_{12}$  and  $\theta_{23}$  for matrix  $m_{III}$  in NH(right) for  $X_2$  condition.

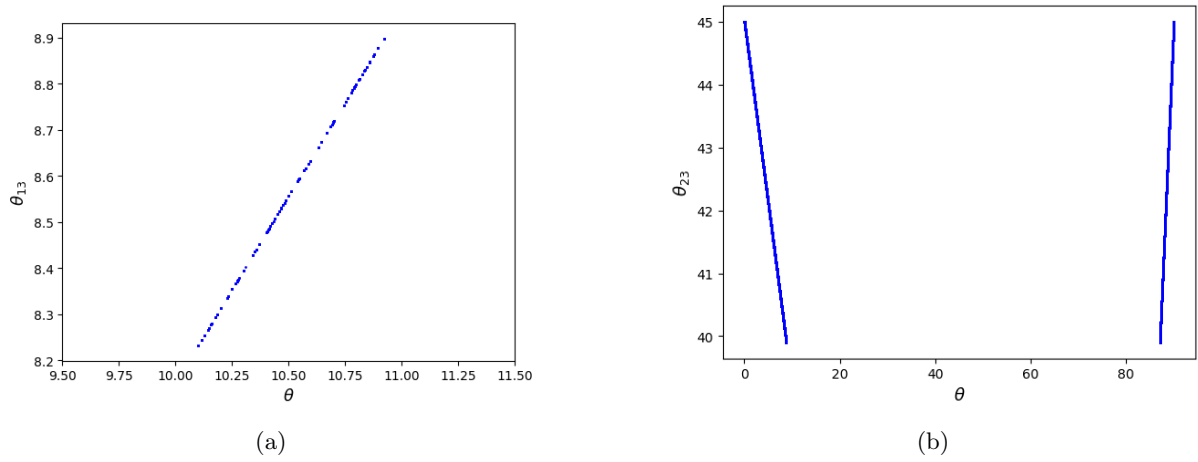


Figure 19: Correlation between mixing angle  $\theta_{13}$  and  $\theta$ (left) and  $\theta_{23}$  and  $\theta$ (right) for  $X_2$  for mass matrix  $m_{III}$  in NH.

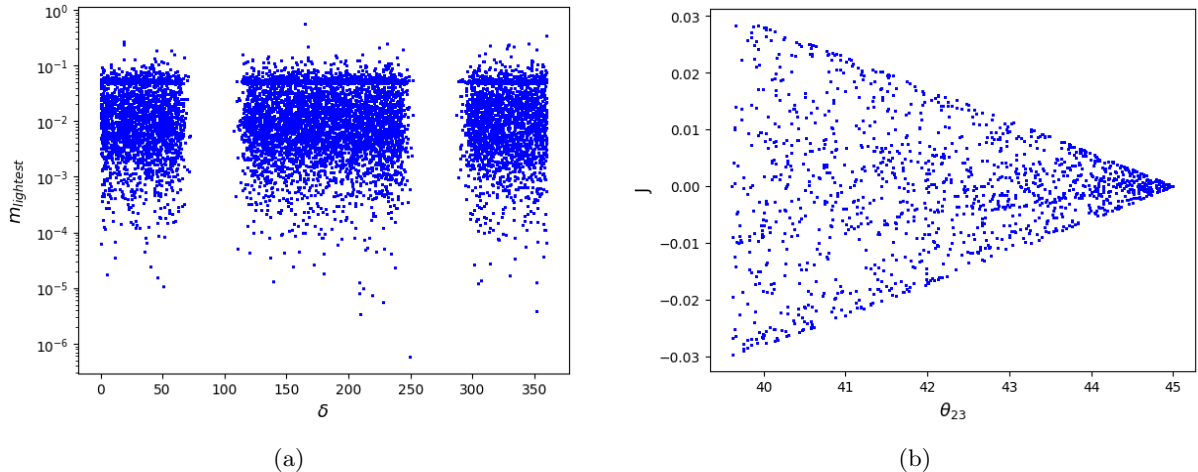


Figure 20: Correlation between  $m_{lightest}$  and  $\delta$ (left) and Jarskog Invariant  $J$  and mixing angle  $\theta_{23}$ (right) for matrix  $m_{II}$  in NH for  $X_2$  condition .

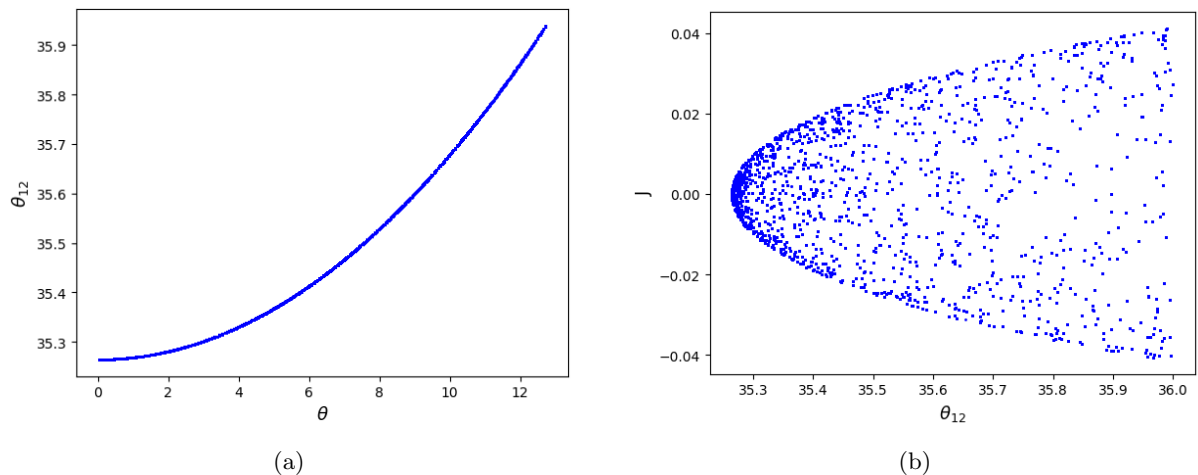


Figure 21: Correlation between  $\theta_{12}$  and  $\theta$  for matrix  $m_{II}$  in NH(left) and  $\theta_{12}$  and  $J$  for matrix  $m_{III}$  in NH(right) for  $X_2$  condition.

## 5 Conclusions

In this paper, we have analyzed the implications of generalized CP symmetries and one zero textures on neutrino mass matrices. We found that the presence of one zero textures, when combined with generalized CP symmetries such as  $X_1$  or  $X_2$ , leads to specific and predictive patterns for the neutrino mass matrix. To obtain the generalized CP conditions, we employed the cTBM matrix, which further constrain the Majorana phases. The presence of one zero textures leads to six distinct patterns for the neutrino mass matrix. For matrices with one zero textures, all cases are allowed except for  $m_I = 0$  in the inverted hierarchy because this condition leads to an excessively large value of reactor mixing angle  $\theta_{13}$ . The presence of the generalized CP conditions in the neutrino mass matrix does not change this property.

All six mass matrices obtained by putting a zero in different positions in the mass matrix follow the conditions imposed by generalized CP symmetry. Generalized CP symmetry is the extended version of CP symmetries, which simply contain more transformations. We computed the effective Majorana mass as a function of the lightest neutrino mass and the sum of the neutrino masses. The results for all the matrices are summarized in Tables 2 and 3. We have calculated the value of the lightest neutrino mass within the constrained region defined by  $R_\nu$  in the  $3\sigma$  range. Additionally, we computed the sum of the three neutrino masses, and by applying the cosmological constraints from Planck data and DESI/SDSS+Pantheon+DES-SN dataset, we found that the

inverted mass hierarchy is disfavored by this data.

Our analysis also shows distinct correlations between the mixing angles and the Dirac CP phase  $\delta$  for the CP symmetries  $X_1$  and  $X_2$ . These correlations serve as identifying features of each texture. In the correlation, we examined the different mixing angles and rotation angle  $\theta$  within their  $3\sigma$  ranges. The resulting correlations illustrate a very constrained region of  $\theta$ . We also present the plots between Jarlskog invariant  $J$  and the mixing angles, which exhibit sharp correlations for both conditions,  $X_1$  and  $X_2$ . Similarly, we investigated the effective Majorana mass as a function of  $\delta$ , which shows compatibility with current experimental data.

Furthermore, we have found that the certain patterns, which have a zero in the off-diagonal position, are not compatible with the cosmological bound provided by Planck data in the  $X_1$  case. Some patterns with zeros in the diagonal positions are similarly incompatible with cosmological constraints in the  $X_2$  case. From the correlation, we find that the rotation angle  $\theta$  is constrained between (14.3 - 15.6) degrees for the  $X_1$  condition, and between (10.1 - 11.1) degrees for the  $X_2$  condition. The neutrino mass matrices in these patterns predict extreme values of  $\theta_{23}$ . Additionally, we note that the complementarity between predictions for  $\theta_{23}$  and  $\delta$  in the one zero textures scenario does not match precisely with current experimental results. Cosmological bounds further constrain the models, with certain patterns, particularly those involving off-diagonal one zero textures, being disfavored by the cosmological data. We also found that specific patterns could be ruled out as more restrictive cosmological bounds on the sum of neutrino masses become available. Overall, the results provide insights into the predictability and testability of neutrino mass matrices that combine one zero textures and generalized CP symmetries.

## Acknowledgements

The authors are thankful to the Inter University Centre for Astronomy and Astrophysics (IUCAA), Pune for providing necessary facilities during the completion of this work.

## References

- [1] M. K. Gaillard, P. D. Grannis and F. J. Sciulli, *Rev. Mod. Phys.* **71**, S96-S111 (1999).
- [2] Y. Fukuda *et al.* [Super-Kamiokande], *Phys. Rev. Lett.* **81**, 1562-1567 (1998).
- [3] Q. R. Ahmad *et al.* [SNO], *Phys. Rev. Lett.* **89**, 011301 (2002).
- [4] K. Eguchi *et al.* [KamLAND], *Phys. Rev. Lett.* **90**, 021802 (2003).
- [5] R. Leitner [Daya Bay], *Nucl. Part. Phys. Proc.* **285-286**, 32-37 (2017).
- [6] J. K. Ahn *et al.* [RENO], *Phys. Rev. Lett.* **108**, 191802 (2012).
- [7] Y. Abe *et al.* [Double Chooz], *Phys. Rev. Lett.* **108**, 131801 (2012).
- [8] G. J. Ding, S. F. King and A. J. Stuart, *JHEP* **12**, 006 (2013).
- [9] I. Esteban, M. C. Gonzalez-Garcia, M. Maltoni, *et al.* *JHEP* **09**, 178 (2020).
- [10] R. N. Mohapatra, S. Antusch, K. S. Babu, *et al.* *Rept. Prog. Phys.* **70**, 1757-1867 (2007).
- [11] K. Abe *et al.* [T2K], *Phys. Rev. Lett.* **112**, 061802 (2014).
- [12] E. Smith [NOvA], *PoS PANIC2021*, 289 (2022).
- [13] C. Giganti, S. Lavignac and M. Zito, *Prog. Part. Nucl. Phys.* **98**, 1-54 (2018).
- [14] M. Tanabashi *et al.* [Particle Data Group], *Phys. Rev. D* **98**, no.3, 030001 (2018).
- [15] X. G. He and A. Zee, *Phys. Rev. D* **84**, 053004 (2011).
- [16] F. Plentinger and W. Rodejohann, *Phys. Lett. B* **625**, 264-276 (2005).
- [17] S. Dev, S. Gupta and R. R. Gautam, *Mod. Phys. Lett. A* **26**, 501-514 (2011).
- [18] Y. H. Ahn, H. Y. Cheng and S. Oh, *Phys. Lett. B* **715**, 203-207 (2012).
- [19] R. Samanta, P. Roy and A. Ghosal, *Eur. Phys. J. C* **76**, no.12, 662 (2016).
- [20] G. J. Ding and J. W. F. Valle, [[arXiv:2402.16963](https://arxiv.org/abs/2402.16963)] [hep-ph].
- [21] P. Chen, C. Y. Yao and G. J. Ding, *Phys. Rev. D* **92**, no.7, 073002 (2015).

- [22] R. R. Gautam, Phys. Rev. D **97**, no.5, 055022 (2018).
- [23] S. Dev, S. Kumar, S. Verma and S. Gupta, Phys. Rev. D **76**, 013002 (2007).
- [24] M. Singh, G. Ahuja and M. Gupta, PTEP **2016**, no.12, 123B08 (2016).
- [25] B. Dziewit, J. Holeczek, M. Richter, et al., Phys. Atom. Nucl. **80**, no.2, 353-357 (2017).
- [26] L. Singh, M. Kashav and S. Verma, Eur. Phys. J. C **82**, no.9, 841 (2022).
- [27] P. H. Frampton, S. L. Glashow and D. Marfatia, Phys. Lett. B **536**, 79-82 (2002).
- [28] S. Dev, L. Singh and D. Raj, Eur. Phys. J. C **75**, no.8, 394 (2015).
- [29] W. Wang, Eur. Phys. J. C **73**, 2551 (2013).
- [30] S. Dev, D. Raj and R. R. Gautam, Phys. Rev. D **96**, no.9, 095002 (2017).
- [31] S. Dev, R. R. Gautam and L. Singh, Phys. Rev. D **88**, 033008 (2013).
- [32] S. Dev and D. Raj, Nucl. Phys. B **957**, 115081 (2020).
- [33] J. Y. Liu and S. Zhou, Phys. Rev. D **87**, no.9, 093010 (2013).
- [34] R. Kalita and D. Borah, Int. J. Mod. Phys. A **31**, no.06, 1650008 (2016).
- [35] S. Dev, S. Verma and S. Gupta, Phys. Lett. B **687**, 53-60 (2010).
- [36] A. Ismael, E. I. Lashin, M. AlKhateeb and N. Chamoun, Nucl. Phys. B **971**, 115541 (2021).
- [37] P. Chen, S. Centelles Chuliá, G. J. Ding, R. Srivastava and J. W. F. Valle, JHEP **03**, 036 (2019).
- [38] S. Kumar and R. R. Gautam, Nucl. Phys. B **1001**, 116520 (2024).
- [39] K. Dick, M. Freund, M. Lindner and A. Romanino, Nucl. Phys. B **562**, 29-56 (1999).
- [40] P. Chen, S. Centelles Chuliá, *et al.* Phys. Rev. D **98**, no.5, 055019 (2018).
- [41] P. Chen, C. C. Li and G. J. Ding, Phys. Rev. D **91**, 033003 (2015).
- [42] Y. Gando [KamLAND-Zen], J. Phys. Conf. Ser. **1468**, no.1, 012142 (2020).
- [43] J. Shirai [KamLAND-Zen], J. Phys. Conf. Ser. **888**, no.1, 012031 (2017).
- [44] J. M. López-Castaño and I. Guinn, PoS **LeptonPhoton2019**, 162 (2019).
- [45] [CUORE], PoS **ICHEP2022**, 552 (2022).
- [46] G. Adhikari *et al.* [nEXO], J. Phys. G **49**, no.1, 015104 (2022).
- [47] M. Aker *et al.* [KATRIN], J. Phys. G **49**, no.10, 100501 (2022).
- [48] N. Aghanim *et al.* [Planck], Astron. Astrophys. **641**, A6 (2020).
- [49] I. J. Allali and A. Notari, [[arXiv:2406.14554](https://arxiv.org/abs/2406.14554) [astro-ph.CO]].